



## Abstract

More so than the traditional fixed radiometers, the scanning radiometer requires a careful design to ensure high quality measurements. Here the impact of the radiometer characteristics (e.g. antenna beam width, receiver bandwidth) and atmospheric propagation (e.g. curvature of the earth and refractivity) on the scanning radiometer measurements are presented. A forward radiative transfer model that includes all these effects to represent the instrument measurements is used to estimate the biases as differences between the measurement with and without these characteristics for three commonly used frequency bands: K, V and W-band. The receiver channel bandwidth errors are not so important in K-band and W-band. Thus, the use of a wider bandwidth to improve detection at low signal-to-noise conditions is acceptable. The impact of the antenna beam width is higher than the receiver bandwidth, but, for V-band where they are of similar importance. Using simple regression algorithms, the effects of the bandwidth and beam width biases in liquid water path, integrated water vapor, and temperature are also examined. The largest errors in liquid water path and integrated water vapor are associated with the beam width errors.

## 1 Introduction

Traditionally, ground-based microwave radiometers have been used in a stand-alone zenith-pointing mode measuring integrated amount of water vapor and liquid water as well as temperature and water vapor profiles (Staelin, 1966; Blaskovic et al., 1987; Güldner and Spänkuch, 1999). Recently, an expansion of the use of scanning radiometers in atmospheric research has been observed. Scanning radiometers have been used in studies of temperature and water vapor in the boundary layer (Martin et al., 2006a; Crewell and Löhnert, 2007; Schween et al., 2011) and in tomographic retrieval of cloud liquid water and water vapor (Huang et al., 2008; Padmanabhan et al., 2009). In particular, co-scanning radar-radiometer measurements are gaining

AMTD

5, 8085–8130, 2012

### Biases caused by MWR characteristics

V. Meunier et al.

Title Page

Abstract

Introduction

Conclusions

References

Tables

Figures

◀

▶

◀

▶

Back

Close

Full Screen / Esc

Printer-friendly Version

Interactive Discussion



**Biases caused by  
MWR characteristics**

V. Meunier et al.

Title Page

Abstract

Introduction

Conclusions

References

Tables

Figures

◀

▶

◀

▶

Back

Close

Full Screen / Esc

Printer-friendly Version

Interactive Discussion



a lot of attraction due to the complimentary nature of their observations. Radars provide information on winds, particle size distributions, precipitation, and cloud, while radiometers will give information on the profiles of temperature and water vapor, and the integrated amount of liquid water content. Thus, the complementary information of these instruments can lead to a better understanding and characterization of clouds (Frisch et al., 1995; Shupe et al., 2008; Saavedra et al., 2012) and thermodynamic profiles (Westwater et al., 1983; Bianco et al., 2003; Gaffard et al., 2006; Löhnert et al., 2008).

Although the advantages of co-scanning radar-radiometers measurements are evident, such observation geometries contain the risks of potential biases in the radiometer measurements due to unaccounted instrument characteristics. For example, at low elevations, the effects of atmospheric refractivity may become an issue. The wide beam widths of the instrument will result in ground emissions data contamination during the lowest elevation scans. Furthermore, the need to maintain scan rates suitable for radar observations will force radiometers to shorten their integration times to keep up with the radar scans, possibly causing increased noise in their measurements. The power received by a radiometer is also proportional to the receiver bandwidth. Thus, the use of a wide receiver bandwidth can result in higher signal-to-noise conditions and thus, shorter integration time that is highly desirable in scanning conditions. However, the use of a wide receiver bandwidth could lead to errors caused by non-negligible changes of the absorption coefficient (equivalently changes in TB) within the bandwidth range.

Han and Westwater (2000) (hereafter HW00) investigated the uncertainty factors of radiometer tipping curves that are used to calibrate K-band channels. In their study, they investigated the impact of earth curvature and antenna beam width for elevation angles ranging between zenith ( $90^\circ$ ) and  $14.5^\circ$ . HW00 report that, for the studied elevation angles, the effect of the vertical gradient of refractive index of air was negligible. They also mentioned that the effect of earth curvature can, for the most part, be corrected. The beam width error increases with width, air mass, and water vapor amount, but corrections can be applied if the antenna side lobes can be neglected. HW00 conclude that tipping data should not include airmass greater than 3, especially

for antenna with beamwidths > 6 deg. Although the study was conducted in the context of microwave radiometer calibration, the issues raised can be applied to the new scanning strategies.

Here, the work of HW00 is expanded by adding lower elevation angles and additional wavelengths that are also widely used in radiometry. First, the forward model framework used in this study is described. Then, the effects that channel bandwidth, antenna beam width, refractive index, and earth curvature have on the measurements of the microwave radiometers and the retrieved atmospheric products are investigated. Finally, a summary of the most important effects will be provided.

## 2 Experimental design

A radiometer instrument model and a forward radiative transfer model are used to study the measurement errors caused by the radiometer's design characteristics and the atmospheric propagation conditions. The input to the radiometer is proportional to the atmospheric radiance  $I$  ( $\text{W m}^{-2} \text{sr}^{-1}$ ) of the incoming radiation in the non-scattering case given by:

$$I(f, \theta) = \int_{\theta'} G(\theta' - \theta) \left[ I_{\text{cos}}(f) \tau(f, 0, \infty) + \int_0^{\infty} \alpha(f, s) e^{-A(f, 0, s)} B(f, T(s)) ds \right] d\theta', \quad (1)$$

where  $\theta$  is elevation angle,  $\theta'$  is the elevation angle of specific ray of the beam,  $G(\theta' - \theta)$  is antenna gain,  $f$  is frequency,  $I_{\text{cos}}$  is the emitted radiation of the cosmic radiating background,  $\tau(f, 0, \infty)$  is the total transmission from top of the atmosphere to the surface,  $s$  is the slant path length,  $\alpha(f, s)$  is the absorption coefficient at  $s$  in  $\text{Np km}^{-1}$ ,  $A(f, 0, s)$  is the absorption between the surface to  $s$ , and  $B(f, T(s))$  is the Planck function with temperature at  $s$ ,  $T(s)$  (i.e. Petty, 2006; Huang et al., 2008). The attenuation calculation performed in the forward model is based on the Rosenkranz (1998) absorption model. This includes the absorption from oxygen, nitrogen and water vapor in the

### Biases caused by MWR characteristics

V. Meunier et al.

Title Page

Abstract

Introduction

Conclusions

References

Tables

Figures

◀

▶

◀

▶

Back

Close

Full Screen / Esc

Printer-friendly Version

Interactive Discussion



atmosphere. The relation between attenuation in dB and that in  $\text{Np km}^{-1}$  is given by:

$$\alpha \left( \frac{\text{Np}}{\text{km}} \right) = -0.2303 \alpha \left( \frac{\text{dB}}{\text{km}} \right). \quad (2)$$

Typically the microwave radiometer measurement is expressed in brightness temperature, TB (in K). Here, brightness temperature is defined by solving the Planck function for temperature as

$$\text{TB} = \frac{hf}{k} \left( \frac{1}{\ln \left( \frac{2hf^3}{l(f, \theta)c^2} + 1 \right)} \right), \quad (3)$$

where  $h$  is Planck's constant and  $k$  is Boltzmann's constant (HW00).

The forward model has three different radio propagation schemes permitting the study of different aspects of the atmospheric propagation. The simplest scheme does not include earth curvature nor the vertical gradient of refractive index. The unit distance travelled through each layer is given by

$$dx = \frac{dh}{\sin \theta}, \quad (4)$$

where  $dh$  is the thickness of the layer and  $\theta$  is the elevation angle (Petty, 2006). The next scheme is typically used in scanning weather radar applications and takes into account the earth curvature effect using the 4/3-earth radius approximation and the standard refractivity profile (Doviak and Zrnica, 2006). In this case,

$$dx = \sqrt{(Ae \sin \varphi)^2 + dh^2 + 2Ae dh - Ae \sin \varphi}, \quad (5)$$

where  $Ae = 4/3 R_e$ ,  $R_e$  is the earth radius, and  $\varphi$  is the entrance angle into the layer. The latter is calculated as

$$\varphi = \sin^{-1} \left( \frac{dx \cos \varphi_0}{Ae} + \sin \varphi_0 \right), \quad (6)$$

**Biases caused by MWR characteristics**

V. Meunier et al.

Title Page

Abstract

Introduction

Conclusions

References

Tables

Figures

◀

▶

◀

▶

Back

Close

Full Screen / Esc

Printer-friendly Version

Interactive Discussion



where  $\varphi_0$  is the preceding exit angle or, for the first layer, the instrument's elevation angle. The final scheme is the most complex and includes both the earth curvature and the actual vertical gradient of the refractive index. The latter is given by

$$\frac{dN}{dh} = \frac{N_j - N_i}{dh}, \quad (7)$$

where  $N_j$  is the refractive index at the top of the layer and  $N_i$  is at the bottom of the layer. The refractive index is calculated following Bean and Dutton (1966)

$$N = \frac{C_p P}{T} + \frac{C_w e}{T^2}, \quad (8)$$

where  $P$  is pressure (in hPa),  $T$  is temperature (in K),  $e$  is vapor pressure (in hPa),  $C_p$  and  $C_w$  are the Bean and Dutton constants ( $C_p = 77.6$ ,  $C_w = 3.75 \times 10^5$ ). More details on the limitations of the constants used in the refractive index can be found in Rüeger (2002). In this propagation scheme,  $dx$  is calculated differently depending on the gradient of refractive index following Eqs. (5) and (6) and exchanging  $Ae$  with

$$F = \frac{1}{\left(\frac{1}{Re} + \frac{dN}{dh}\right)}. \quad (9)$$

Detailed comparisons of the forward model output from the three different propagation schemes and for different frequency bands will be used to quantify the errors caused by omitting only the refractive index and/or the earth curvature.

In addition to radio propagation, the forward model also takes into account the antenna beam width and the channel bandwidth of the radiometer. Typical antenna patterns of radiometer systems show a Gaussian shape and a sidelobe suppression of better than  $-30$  dB. Therefore, the beam width calculation is done using a Gaussian quadrature following Huang et al. (2008) neglecting the effects of the sidelobes. The evaluation of the beam width is one dimensional in the elevation axis. This assumes

**Biases caused by MWR characteristics**

V. Meunier et al.

Title Page

Abstract

Introduction

Conclusions

References

Tables

Figures

◀

▶

◀

▶

Back

Close

Full Screen / Esc

Printer-friendly Version

Interactive Discussion



**Biases caused by  
MWR characteristics**

V. Meunier et al.

[Title Page](#)[Abstract](#)[Introduction](#)[Conclusions](#)[References](#)[Tables](#)[Figures](#)[◀](#)[▶](#)[◀](#)[▶](#)[Back](#)[Close](#)[Full Screen / Esc](#)[Printer-friendly Version](#)[Interactive Discussion](#)

an axis-symmetric beam pattern that excludes the azimuthal effects inside the beam. Azimuthal scanning is not implemented in the model and thus, a horizontally homogeneous atmosphere is assumed. In the case where the beam partially hits the ground, the radiances of that part of the beam are changed to the blackbody radiances emitted by the ground represented by the lowest level in the soundings. In reality this contribution will depend on the actual position of the radiometer and the emissivity from different ground cover types. The receiver bandwidth modeling is achieved by subdividing the bandwidth into a series of discrete frequencies that are used in the forward model. The radiances are calculated for each of these frequencies and then, they are simply integrated to create the effect of channel bandwidth. In this study, the shape of the bandwidth is idealized to a “square” filter. However, this could easily be changed to other filter shapes, once they are known, by changing the weights of each of the radiances. This is important, as in reality the specified center frequency does not necessarily correspond to the bandwidth filter shape averaged frequency (Crewell et al., 2001).

The radiometer characteristics used for this study are chosen from the designs of commercially available and experimental instruments. The group of instruments used to create these ranges is listed in Table 1. The frequencies incorporated in the model are the traditional frequencies in K-band (here 15 to 35 GHz) and V-band (here 50–60 GHz). The K-band covers the 22.235 GHz water vapor absorption line providing information on the amount of liquid water and water vapor (Fig. 1). The V-band dominated by the 60 GHz oxygen absorption band that provides information on the temperature distribution in the atmosphere. In addition, the W-band (94 GHz) frequencies are also added because they are strongly sensitive to liquid water signal and are widely used in the millimeter wavelength radar community, being interesting for possible radar-radiometer synergetic measurements. This frequency band is also used in radiometry. The Department of Energy’s (DOE) Atmosphere Radiation Measurement (ARM) Climate research Facility has added 3-channel radiometers that include the 90 GHz to several of their sites (Voyles, 2012). ARM also uses the Radiometer Physics GmbH (RPG) dual-frequency radiometer that works at 90 GHz and 150 GHz (Cadeddu, 2011).

**Biases caused by  
MWR characteristics**

V. Meunier et al.

Title Page

Abstract

Introduction

Conclusions

References

Tables

Figures

◀

▶

◀

▶

Back

Close

Full Screen / Esc

Printer-friendly Version

Interactive Discussion



In this study, we examine 201 K-band frequencies, 101 V-band frequencies and 56 W-band frequencies with each frequency being separated by 0.1 GHz. The beam widths chosen range from 0.5° to 10°, while the channel bandwidths range between 100 MHz and 1000 MHz. These settings cover the specifications of current microwave instruments. The elevation angles from 0.5° to 90° are chosen to emphasize the low elevation scans required when performing boundary layer scans or when scanning with radars. The latter usually scan low to the horizon in order to be able to detect hydrometeors in the boundary layer at a distance. HW00 used elevation starting at 14.5° in their work on tipping curve calibrations. We included some of these higher elevation angles for the sake of comparison, as well as indication for the radiometers that still use the traditional high elevation scans. A summary of the instrument characteristics used in this study can be found in Table 2.

A simple retrieval algorithm is used to calculate the response of certain retrieved atmospheric parameters to the errors for both K-band and V-band. The parameters that were derived are integrated water vapor (IWV), liquid water path (LWP), and temperature ( $T$ ). Both the IWV and LWP are derived using only the 23.8 GHz and 31.4 GHz K-band frequencies for elevation angles 90, 42, 30, 19.2, 10.2, and 5.4°. The W-band was not included in the algorithm, although an improvement of 50% can be made using the 90 GHz frequency in LWP retrievals because of its sensitivity to clouds (Crewell and Löhnert, 2003). Both the LWP and the IWV are derived from quadratic regressions. The LWP was derived from TB measurements as

$$\text{LWP} = \sum_i c_0 + c_1 \text{TB}_i + c_2 \text{TB}_i^2, \quad (10)$$

where  $\text{TB}_i$  is the brightness temperature defined previously in Kelvin for each frequency,  $i$ , and  $c_0$ ,  $c_1$ , and  $c_2$  are the regression coefficients (Löhnert and Crewell, 2003). The same equation is used for the IWV regression, but the regression coefficients are different. All statistical errors refer to the path integrated amounts and are not mapped to zenith values. The temperature profiles retrieval is based on 7 V-band frequencies (51.26, 52.28, 53.86, 54.94, 56.66, 57.3, and 58 GHz) where the first 3

frequencies are used only in zenith pointing and the last 4 consider all the elevations angles used for the IWV and LWP retrievals. The temperature was derived using a linear regression from TB measurements as

$$T = d_0 + d_1 TB_j, \quad (11)$$

where  $d_0$  and  $d_1$  are the regression coefficients (Crewell and Löhnert, 2007).

The standard mid-latitude summer and winter atmospheric profiles from McClatchey et al. (1971) are used to describe the atmospheric structure and properties (Fig. 2). The soundings are treated as climatological standards and representative of the typical conditions encountered in areas where radar-radiometer systems operate and cover two different climate regimes: the warm moist summer and the dry cold winter. However, it is to be noted that some results are sounding dependent such as the some of the bandwidth errors. Therefore, some of the effects mentioned here will dependent on the atmospheric situation. Both of these soundings are clear air profiles and do not contain cloud liquid water.

### 3 Analysis

In this section, each of the radiometer instrument characteristics will be examined individually. An interpretation of their observed biases will be provided along with an assessment on their impact on the retrieved geophysical parameters of interest. The results will be shown as errors in TB. The bias errors are defined as

$$TB_{\text{error}} = TB_{\text{assumption}} - TB_{\text{reality}}. \quad (12)$$

The assumption is defined as being the approximation of the idealized radiometer generally used in forward models where antenna beam width and channel bandwidth are considered to be delta functions. The reality includes the width of either the bandwidth or the beam width. The effects are studied individually meaning that when the bandwidth is studied the beam width is neglected and vice versa for the beam width studies.

## Biases caused by MWR characteristics

V. Meunier et al.

Title Page

Abstract

Introduction

Conclusions

References

Tables

Figures

◀

▶

◀

▶

Back

Close

Full Screen / Esc

Printer-friendly Version

Interactive Discussion



## 3.1 Receiver bandwidth effect

### 3.1.1 K-band simulations

In K-band, the TB curvature changes are caused by the water vapor absorption line at 22.235 GHz (Fig. 1). The most prominent feature in the error analysis is a dipole of under and over estimation that is associated with this absorption peak (Fig. 3). The area of under-estimation on the low frequency side of the absorption peak is associated to the negative curvature associated to the low frequency wing of the absorption peak where the atmosphere is most transparent (Fig. 4). This leads to an under-estimation of TB if the delta-function bandwidth approximation is used. The maximum value of the under-estimation is  $-0.7\text{K}$  at an elevation of  $14^\circ$  for a bandwidth of 1 GHz in the summer sounding (Fig. 3). The area of over-estimation is associated to the positive curvature of the absorption peak which is linked to the atmosphere being more opaque (Fig. 4). The maximum value of the over-estimation occurs at elevations between  $12^\circ$  and  $14^\circ$  for the largest bandwidth and is of  $1.8\text{K}$  again with the summer sounding (Fig. 3). As expected, the largest errors are linked to the largest bandwidths. For bandwidths less than 200 MHz, the errors caused by the bandwidth approximation are negligible and can be ignored. At the lowest elevation angle used in this study ( $0.5^\circ$ ) the location of the dipole has shifted to lower frequencies. This shift is caused by the broadening of the water vapor absorption peak at low elevation angles (Fig. 4) displacing the curvature changes that cause the errors. There are differences in the errors caused by the bandwidth approximation between the mid-latitude summer and winter soundings. The maximum errors values in the winter (summer) sounding are of  $1.5\text{K}$  ( $1.8\text{K}$ ) for the over-estimation and of  $-0.6\text{K}$  ( $-0.8\text{K}$ ) for the under-estimation. The widths in frequency of the over-estimation and under-estimation areas depend on the atmospheric structure and the winter sounding exhibits the narrowest widths. These are mainly caused by the increase of water vapor in the summer sounding. The difference between the soundings shows that these results are sounding dependent. The curvature of the TB spectrum (Fig. 4) lead to areas of over-estimation and under-estimation

## Biases caused by MWR characteristics

V. Meunier et al.

Title Page

Abstract

Introduction

Conclusions

References

Tables

Figures

◀

▶

◀

▶

Back

Close

Full Screen / Esc

Printer-friendly Version

Interactive Discussion



**Biases caused by MWR characteristics**

V. Meunier et al.

Title Page	
Abstract	Introduction
Conclusions	References
Tables	Figures
◀	▶
◀	▶
Back	Close
Full Screen / Esc	
Printer-friendly Version	
Interactive Discussion	



errors, which has an impact on the retrieval's solutions. The K-band measurements are used in retrievals to determine the IWV and LWP of the atmosphere. The errors for both retrieved parameters are more important at low elevations angles for the summer sounding at the largest bandwidths (Fig. 5). For IWV, the largest errors are  $-0.7 \text{ kg m}^{-2}$  ( $-0.5 \text{ kg m}^{-2}$ ) at  $10^\circ$  elevation with the summer (winter) sounding for the largest bandwidth. For both soundings, the errors in IWV decrease with increasing elevation angle to become negligible for zenith pointing instruments. For LWP, the errors due to channel bandwidth are below  $1 \text{ g m}^{-2}$  for all settings and can be neglected. The reason is the strong impact of the 31.4 GHz channel used in the retrieval that is located in a window region.

**3.1.2 V-band simulations**

Absorption in the V-band is caused by the oxygen complex (Fig. 1) which consists of several closely spaced absorption lines. Because of pressure broadening the individual lines only significantly appear within the spectrum under low pressure conditions. With increasing opacity, i.e. low elevation angles and/or high frequency, the V-band channels become saturated and thus, any change in TB caused by the bandwidth approximation will have negligible effect. For this reason, frequencies above 55 GHz at all elevation angles are saturated (Fig. 6). Starting at  $4^\circ$ , an area of over-estimation moves up in frequency as the elevation angle increases (50 GHz at  $4^\circ$  to 53 GHz at  $30^\circ$ ) (Fig. 7). This area of over-estimation is attributed to the positive curvature of the TB spectrum ahead of the saturation around 55 GHz (Fig. 6). This is associated to opaque frequencies that receive their entire signal from close ranges from the lower atmosphere. The maximum value of the over-estimation in TB is 1.5 K at elevations between  $30^\circ$  and  $90^\circ$  for the widest bandwidth (Fig. 7). This will lead the retrieval algorithms to slightly over-estimate the temperature at low altitudes. The largest error in the retrieved low-level temperature is an over-estimation of 0.1 K for the largest bandwidth (Fig. 8). Starting at  $6^\circ$  elevation, the opposite effect is observed to the left of the over-estimation. The area of under-estimation widens as the elevation increases. This under-estimation is associated to

**Biases caused by  
MWR characteristics**

V. Meunier et al.

Title Page

Abstract

Introduction

Conclusions

References

Tables

Figures

◀

▶

◀

▶

Back

Close

Full Screen / Esc

Printer-friendly Version

Interactive Discussion



the negative curvature of the TB spectrum (Fig. 6). This inflection is caused by the absorption reaching the values associated to the edge of the absorption peak at the most transparent frequencies and are linked to higher altitudes in the atmosphere. Therefore, this will tend to under-estimate the temperature at mid-level altitudes in the atmosphere. The maximum value of the under-estimation in TB is  $-0.6$  K at elevations between  $20^\circ$  and  $30^\circ$  for the widest bandwidth (Fig. 7). The largest error in the retrieved mid-level (4 km) temperature is an under-estimation of  $-1.8$  K for the largest bandwidth (Fig. 8).

In the case that the receiver bandwidth is small enough, the effects of the individual oxygen absorption peaks will become apparent. This is indicated by the presence of striations at elevations above  $4^\circ$ . The striations are seen as alternating over-estimations in TB, with maximum around  $7.9$  K, and under-estimations, with minimums around  $-2$  K, at an elevation of  $90^\circ$  for the widest bandwidth using the summer sounding (Fig. 7). The striations are not so noticeable at angles below  $6^\circ$ , because of the saturation of the low elevation angles that mask most of them. Each of the oxygen absorption peaks have areas of over-estimation and under-estimation associated with the absorption peak as seen with the K-band's single peak. The choice of the resolution is most challenging for the V-band due to these multiple absorption peaks. In order to take into account the individual effect of each line, the resolution would need to be much finer than the minimum of  $100$  MHz used here. Most radiometers do not resolve every individual line. Therefore, it is important that the radiometer's center frequencies and bandwidth are chosen to be between these oxygen peaks, as is done with the HAT-PRO instrument (Fig. 9). The individual peaks will have an effect on the errors caused by the radiometers bandwidth in V-band. The magnitude of the error will depend on the size of the bandwidth considered. The peaks can be either averaged out at large bandwidth or detected individually at narrower ones. Here, the bandwidths are calculated for each frequency independently and are plotted. It is for this reason that the striations are not smeared at wider bandwidths. These effects are not seen in K-band as it is a single peak, nor are they seen in W-band, which is a window region in the

absorption spectrum. The only small difference between the mid-latitude summer and winter soundings is the magnitude of the errors caused by the bandwidth approximation. The maximum errors in TB are of 6.5 K for the over-estimation and -1.9 K for the under-estimation in the winter sounding at an elevation of 90° for the 1 GHz bandwidth.

5 This shows a difference of error in TB on the order of 1.5 K for the over-estimation between these soundings and no difference are seen in the under-estimation errors.

### 3.1.3 W-band simulations

In W-band, the TB frequency curvature at any given angle is highly linear (no absorption peaks) due to the fact that this frequency band is an atmospheric window region (Fig. 1). Therefore, the channel bandwidth frequencies errors are negligible. Window regions are not interesting for radiometric profiling, because some variation of absorption with frequency is needed to be able to obtain height-resolved information. Thus, only integrated amounts will be possible as the slope does not seem strong enough for sounding (ranging) techniques. This band is the most sensitive to cloud liquid water of the three bands examined here because cloud absorption increases as the square of the frequency (Fig. 1). Thus, it is well suitable to provide information on low LWP in the atmosphere (Crewell and Löhnert, 2003).

The question of the channel bandwidth is particularly important for radar-radiometer synergy, because of the link between integration time and bandwidth. The theoretical precision of the radiometer is given by

$$\Delta T \propto \frac{(T_N + T_A)}{\sqrt{B\tau}}, \quad (13)$$

where  $T_N$  is the instrument's noise temperature,  $T_A$  is the measured TB,  $B$  is the channel bandwidth, and  $\tau$  is the measurement integration time (Ulaby et al., 1981). The noise temperature is an instrument dependent constant. From Eq. (14) is is apparent that the product of receiver bandwidth and integration time controls the radiometer sensitivity. If the radar and radiometer systems are on the same scanner and the scan

## Biases caused by MWR characteristics

V. Meunier et al.

Title Page

Abstract

Introduction

Conclusions

References

Tables

Figures

◀

▶

◀

▶

Back

Close

Full Screen / Esc

Printer-friendly Version

Interactive Discussion



rate is determined by the radar scan strategy, the radiometer integration time will be very short compared to traditional ground-based radiometer systems. Thus, in order to maintain or improve the radiometer sensitivity under such operational constraints, it is necessary to increase the receiver bandwidth. For a radiometer with a bandwidth of 100 MHz and integration time of 1s, the sensitivity will be 0.2 K, while at radar integration times (1/30 s) it will be of 1.2 K. But if the bandwidth is increased to 1 GHz, it will be 0.4 K. Note that the sensitivity of the radiometer causes a statistical error around the true value unlike the other errors mentioned in this paper which are biases.

## 3.2 Antenna beam width effect

### 3.2.1 K-band simulations

In K-band, the errors introduced by the antenna beam width approximation can be substantial, especially at low elevation angles, compared to those caused by the channel bandwidth approximation. The errors in over-estimation are of 13.2 K at an elevation of  $4^\circ$  for the  $10^\circ$  beam width and of  $-40.3$  K at the same elevation for the same beam width in under-estimation and are larger at lower elevations (Fig. 10). At elevation angles below  $8^\circ$ , the over-estimation errors are present at the peak, which is not the case with higher elevation angles where only under-estimation is present (Fig. 10). At these elevations, the frequencies at absorption peak are associated to a positive curvature of the TB dependency with angle, associated to an over-estimation of TB, because they are optically thick and near saturation (Fig. 11). The frequencies at the wing of the peak are more transparent and thus are associated to the negative curvature of the TB dependency with angle associated to an under-estimation of TB. At elevations above  $8^\circ$ , the frequencies are all somewhat transparent to the atmosphere and as such they have a negative curvature. Above  $20^\circ$  elevation, the opaque absorption peak is now linked to the larger under-estimation values and the transparent wings to area of smaller values. At these elevations, the transparent frequencies show little curvature while the less transparent frequencies still have some negative curvature affecting

## Biases caused by MWR characteristics

V. Meunier et al.

Title Page

Abstract

Introduction

Conclusions

References

Tables

Figures

◀

▶

◀

▶

Back

Close

Full Screen / Esc

Printer-friendly Version

Interactive Discussion



**Biases caused by  
MWR characteristics**

V. Meunier et al.

[Title Page](#)[Abstract](#)[Introduction](#)[Conclusions](#)[References](#)[Tables](#)[Figures](#)[◀](#)[▶](#)[◀](#)[▶](#)[Back](#)[Close](#)[Full Screen / Esc](#)[Printer-friendly Version](#)[Interactive Discussion](#)

them (Fig. 11). The magnitude of the errors decreases with increasing elevation angle to become negligible for zenith pointing instruments. This is as expected since the difference of including off-zenith measurements in the beam width is less important than the inclusion of the more strongly emitting lower angles at low elevation. Just like with the bandwidth, the errors are sounding dependent. The magnitude of the errors are different in winter with a maximum over-estimation of  $-0.8$  K at  $4^\circ$  elevation for the widest beam width and  $-34.5$  K under-estimation at  $4^\circ$  elevation for the same beam width. Here also, the areas of over-estimation and under-estimation errors cause a change in the TB dependency with angle shape, which has an impact on the retrieval's solutions. The errors in beam width have a larger impact on the retrieved parameters I WV and LWP than those seen with the bandwidth errors. For I WV, the largest errors occur at the widest beam width and for the lowest elevation angles ( $10^\circ$ ) where errors of  $7.9$   $\text{kg m}^{-2}$  are seen using the winter sounding and  $5.3$   $\text{kg m}^{-2}$  for the summer sounding (Fig. 5). For elevation angles of  $30^\circ$ , the errors at these beam width drop to  $1$   $\text{kg m}^{-2}$  for summer and  $0.2$   $\text{kg m}^{-2}$  in winter. For LWP, the summer sounding has more important errors,  $32$   $\text{g m}^{-2}$  at  $10^\circ$  elevation for  $10^\circ$  beam width, than the winter sounding,  $9$   $\text{g m}^{-2}$  for the same elevation and beam width. The errors in LWP drop to below  $1$   $\text{g m}^{-2}$  above  $30^\circ$  elevation for all beam widths.

### 3.2.2 V-band simulations

The errors related to the antenna pattern have similar magnitude to those associated with the channel bandwidth. The simulations indicate that at frequencies above 55 GHz, the wavelengths are saturated and therefore no errors due to the antenna pattern are present (Fig. 12). The maximum values are of 8 K over-estimation at the  $4^\circ$  elevation angle and an under-estimation of  $-2.2$  K at a  $20^\circ$  elevation angle, both for the  $10^\circ$  beam width. At elevation below  $10^\circ$ , an area of over-estimation occurs at the most transparent frequencies (50–52 GHz) and are linked to the positive curvature of the TB curve (Fig. 13). This curvature is caused by the frequencies transparent enough to be affected by the beam width and by the fact that as the elevation angles get higher the

atmosphere becomes less opaque. At low elevation angles, even the most transparent frequencies don't travel far through the atmosphere. Therefore, at the low elevation angles, the low altitude atmospheric temperature will tend to be over-estimated. Between elevation angles of 12° and 30°, an area of under-estimation appears to the left of the area of over-estimation (Fig. 13). At elevations above 30°, the area of over-estimation disappears completely and the area of under-estimation widens to include all frequencies below 55 GHz (Fig. 13). The errors become smaller with increasing elevation angle. The largest error in TB at these elevations is of 0.6 K for the widest beam width at 45°. The retrieval shows an over-estimation of 0.2 K for the widest beam width at mid-level in the atmosphere in both soundings (Fig. 14). The error magnitudes and the areas of under-estimation and over-estimations are similar in both soundings. The maximum value of over-estimation in TB in the winter profile is of 8 K at an elevation of 4° for the widest beam width and of -2.2 K for the under-estimation at an elevation of 20°. Therefore, the effect does not seem to be sounding dependent.

### 3.2.3 W-band simulations

In W-band, the effect of antenna beam width, unlike the receiver channel bandwidth, is not negligible. The errors are an over-estimation of 10.9 K for a beam width of 10° at an elevation of 4° and an under-estimation of -2.9 K at an elevation of 14° and are higher at low elevation angles (Fig. 15). At these elevations, the TB curve shows a positive curvature and the amount of curvature increases with increasing beam width. The positive curvature is linked to the low elevation angles being near saturation. Above 12° elevation, there is a gradient from negligible error to under-estimation at large beam width. Here, the TB curve shows a negative curvature and the amount of curvature increases with increasing beam width. The negative curvature is linked to the higher angles passing through more transparent layers in the atmosphere. At elevations above 45°, the errors drop below -0.6 K, because the curvature of the TB curve is reduced. There are some differences between the mid-latitude summer and winter soundings with the magnitude of the errors being larger in the winter sounding. As mentioned

## Biases caused by MWR characteristics

V. Meunier et al.

Title Page

Abstract

Introduction

Conclusions

References

Tables

Figures

◀

▶

◀

▶

Back

Close

Full Screen / Esc

Printer-friendly Version

Interactive Discussion



**Biases caused by  
MWR characteristics**

V. Meunier et al.

[Title Page](#)[Abstract](#)[Introduction](#)[Conclusions](#)[References](#)[Tables](#)[Figures](#)[◀](#)[▶](#)[◀](#)[▶](#)[Back](#)[Close](#)[Full Screen / Esc](#)[Printer-friendly Version](#)[Interactive Discussion](#)

previously, W-band is very sensitive to the presence of clouds and thus these errors will cause the retrieval algorithm to change the LWP. Thus the retrieval might compensate the over-estimation (under-estimation) by adding (subtracting) liquid water amounts in the atmosphere if there is no other piece of information (e.g. lidar, radar or other radiometer channels such as K-band) to help locate the presence of liquid water.

Blahak (2008) has studied the effect of the elongation of the beam caused by averaging over several measurements while scanning. Although this was derived for radar, this effect would present in scanning radiometers measurement if the radiometer does not stare during the collection of data. In a stand-alone mode, the instrument could stop at any given angle to collect a series of measurement and then continue to the next angle as such the dwell time and elongation are not an issue. However, when radiometers co-scan with radars, the dwell time required to follow the radar is very short. Thus, the radiometer must take near continuous measurements and the problem of elongation appears. Another issue is the beam matching between the instruments. It is important to note that the beam width will depend on frequency. Higher frequencies have narrower beam width. Therefore, when using instruments with different frequencies, beam matching will have to be taken into account. In the case of radar and radiometer sharing the same antenna, the radar antennas are not quite suitable for radiometric use. Radiometers require antennas with very little side lobes, so that the measurement is not contaminated by radiation incoming from different sources. This problem is more important for radiometer than for radar because the radar signal is 2-way, which reduced the side lobes by the square, while the radiometer, being only 1-way, does not. The antenna must be made from materials that are non-absorbent, because the emission from the antenna will be mixed to the emission from the atmosphere creating additional errors.

### 3.3 Refractive index effect

The refractive index error is calculated as the difference between the TB calculated by the forward model using the full propagation (Eqs. 5 and 9) and the TB calculated by

**Biases caused by  
MWR characteristics**

V. Meunier et al.

[Title Page](#)[Abstract](#)[Introduction](#)[Conclusions](#)[References](#)[Tables](#)[Figures](#)[◀](#)[▶](#)[◀](#)[▶](#)[Back](#)[Close](#)[Full Screen / Esc](#)[Printer-friendly Version](#)[Interactive Discussion](#)

the forward model using the propagation with 4/3-earth radius approximation (Eq. 5). The impact of the vertical gradient of the refractive index of air on the radio propagation depends on the assumed atmospheric structure. Here, climatological soundings represent an average for a certain climate zone and extreme refractive index profiles are not included. A more comprehensive study will need to use a large number of soundings capturing the variability of the vertical gradient of the refractive index. The propagation errors are more important at low elevations. In the case of the refractive index, the lower elevation angles are most affected because the radiation must travel longer through a thicker part of the atmosphere and will be bent more while at 90° there will be no effect. The main quantities affecting the change of refractive index are pressure, temperature and water vapor (Eq. 8).

The simulated errors at K-band are larger than the errors of the other frequency bands (V and W). The saturation of the V-band and W-band frequencies causes the TB to be less sensitive to the change of the beam altitude due to the refractive index. Thus, the errors at these frequencies are negligible. The errors in K-band are over-estimations with the summer sounding and under-estimations with the winter sounding (Fig. 16). The errors are of 2.6 K at 4° elevation in summer and -1.6 K at the same elevation angle in winter and are larger at lower elevation angles. The effect is more important in the low frequencies where the atmosphere is more transparent and travels further. At elevations above 8°, the effects are negligible for all frequency bands, as found by HW00 for K-band.

**3.4 Earth curvature effect**

The earth curvature errors are calculated as the difference between TB calculated by the forward model using propagation without earth curvature (Eq. 4) and the TB calculated by the forward model using propagation with 4/3 earth radius (Eq. 5), which includes the earth curvature. The effect of earth curvature on the radiometer measurement causes under-estimation at all frequencies. The amount of under-estimation depends on the frequency band with K-band having the largest errors and V-band the

**Biases caused by  
MWR characteristics**

V. Meunier et al.

Title Page

Abstract

Introduction

Conclusions

References

Tables

Figures

◀

▶

◀

▶

Back

Close

Full Screen / Esc

Printer-friendly Version

Interactive Discussion



smallest. Since the K-band frequencies are not saturated, the effect caused by the change of height of the beam due to the earth curvature will affect the measurement of TB (Fig. 16). This effect will cause smaller changes in the beam height at frequencies that are near saturation, such as V-band and W-band. This effect is also elevation angle dependent. At high elevation angles, whether the earth is spherical or flat changes very little the height at which the beam is pointing. At low elevation angles, the earth curvature increases the height above ground at which the instrument points. Thus, the effect is most pronounced at low elevation angles, less than  $6^\circ$ , with the lowest angle being the most strongly affected.

For K-band, the lowest elevation angles seem to show a larger effect on the low-frequency wing. Above  $4^\circ$ , the effect becomes symmetrical on both wings. The absorption peak being saturated shows little effect. The errors are much larger in the winter sounding. This is caused by the frequencies being less saturated in the colder drier winter sounding. The error is  $-5.5\text{ K}$  at an elevation of  $4^\circ$  in summer and  $-6.3\text{ K}$  at the same elevation in winter and again are larger at lower elevations. HW00 found that the effects are still relatively important at higher elevation angles. They also offer a correction to minimize this effect. The under-estimation errors will cause an under-estimation of IWV and LWP in the retrievals. For V-band, there is also an under-estimation. At these frequencies, two effects come into play the first, and most important, is saturation. This is the reason why the lower elevation angles to show no change. The more opaque frequencies ( $> 53\text{ GHz}$ ) are saturated and an apparent change in elevation angles will have little effect. For the more transparent frequencies, the effect of the change of altitude of the beam caused by the earth curvature will be more important. When not saturated, this effect is more important at elevation angles up to  $30^\circ$  in elevation and no changes are seen at zenith. The errors are very similar between the two soundings. The maximum error in summer is  $-1.1\text{ K}$  between  $6^\circ$  and  $8^\circ$  in elevation and  $-1.2\text{ K}$  in winter at the same elevations. The retrieval will cause an under-estimation of the temperature profile at all levels in the atmosphere. As with the V-band, the W-band also has the saturation and the earth curvature effect competing with each other. At very

**Biases caused by  
MWR characteristics**

V. Meunier et al.

Title Page

Abstract

Introduction

Conclusions

References

Tables

Figures

◀

▶

◀

▶

Back

Close

Full Screen / Esc

Printer-friendly Version

Interactive Discussion



low elevations angles, the saturation effects are dominant. At less opaque elevation angles, it is the height difference cause by the earth curvature that is dominant up to a certain point where, at higher elevation angles, the effect is too small. The most affected angles are found at elevation angles up to  $30^\circ$ . Here again, the errors are more important in the winter sounding than in the summer one. The maximum errors are  $-0.9\text{ K}$  in summer at elevation of  $6^\circ$  and  $-5.8\text{ K}$  at  $2^\circ$  in the winter. These errors will also cause the retrieval to under-estimate the LWP.

**4 Summary**

This study investigates the bias errors introduced to scanning radiometer measurements related to the instrument's receiver bandwidth (100–1000 MHz), antenna beam width, ( $0.5\text{--}10^\circ$ ), atmospheric refraction, and earth curvature (Table 2). The causes of the errors were determined and their effects on the retrieved atmospheric parameters Integrated Water Vapor (IWV), Liquid Water Path (LWP), and temperature profile were also examined for three frequencies bands. The errors were defined as differences in brightness temperature (TB) between the forward model approximations that does not account for the instruments characteristics,  $TB_{\text{assumption}}$  (or in the case of the refractivity and earth curvature study the simplest form) and a forward model that would have all these characteristics included,  $TB_{\text{reality}}$  (more complex formulation). Depending on the curvature of the TB curve, positive or negative TB errors are found. Areas with positive curvature will cause  $TB_{\text{assumption}}$  to be over-estimated compared to  $TB_{\text{reality}}$ , while areas with negative curvature will be responsible for the under-estimation of  $TB_{\text{assumption}}$  with respect to  $TB_{\text{reality}}$ . In general, larger the biases are associated to larger the beam width and bandwidth.

At K-band (15–35 GHz), the effect of the bandwidth is small. The largest errors (1.8 K) were associated with an over-estimation around the absorption peak (Table 3). The beam width effect yields larger errors. The under-estimation linked to the absorption peak has errors of  $-40.3\text{ K}$ , while the over-estimation is around 13.2 K at an elevation

of  $4^\circ$  both in summer (Table 3). Large errors are found at low elevation angles, below  $10^\circ$ . These lead to errors in the retrieved integrated atmospheric quantities of IWV and LWP that are much larger in beam width (IWV  $7.9 \text{ kg m}^{-2}$  and LWP  $31.7 \text{ g m}^{-2}$ ) than in bandwidth (IWV  $0.7 \text{ kg m}^{-2}$  and LWP  $< 1 \text{ g m}^{-2}$ ) just as with the TB errors (Table 4).

As the elevation angles increases, the errors decrease until they become negligible above  $30^\circ$ . The main challenge in the V-band (50–60 GHz) are the errors caused by the absorption peaks making up the oxygen complex. These absorption peaks cause under-estimation errors and over-estimation errors depending on the TB spectrum's curvature. The under-estimation can be as large as  $-2 \text{ K}$  and the over-estimation range around  $8 \text{ K}$  (Table 3). Therefore, it is important to choose the V-band frequencies between the absorption peaks to reduce the errors. If the frequencies are placed between these absorption peaks and are used at low elevation angles, the errors in bandwidth are smaller. The errors on the retrieved temperature profile caused by the errors in TB by the channel bandwidth are negligible at low levels and become an under-estimation of  $-1.8 \text{ K}$  at mid-levels (Table 4). The beam width errors are largest at low elevation angles, where an over-estimation of  $8 \text{ K}$  is found at the low frequencies (Table 3). At elevations above  $20^\circ$ , the errors become under-estimations at these frequencies, but these errors are smaller with a maximum around  $-2.3 \text{ K}$ . The errors on the retrieved temperature profile cause by the errors in TB by the antenna beam width are over-estimation of  $0.2 \text{ K}$  at mid-levels and become under-estimation of  $-0.1 \text{ K}$  at low levels (Table 4). In W-band (90–95 GHz), the errors related to the beam width are the most important especially at elevation angles below  $14^\circ$ . At elevation below  $8^\circ$ , the errors are over-estimation with error such as  $11 \text{ K}$  in summer and  $3.6 \text{ K}$  in winter at  $4^\circ$  that are larger at low elevation in winter (Table 3). At higher elevations, the errors turn to under-estimation with the largest errors around  $-9.3 \text{ K}$  in winter and  $-2.9 \text{ K}$  in summer (Table 3). These errors become negligible above  $45^\circ$  in elevation. The bandwidth effects are also negligible because there is no absorption peak (Table 3). W-band frequencies are very sensitive to cloud liquid water so the errors are going to affect the LWP retrievals. For the effect of vertical gradient of the atmospheric refractive index,

**Biases caused by  
MWR characteristics**

V. Meunier et al.

Title Page

Abstract

Introduction

Conclusions

References

Tables

Figures

◀

▶

◀

▶

Back

Close

Full Screen / Esc

Printer-friendly Version

Interactive Discussion



**Biases caused by  
MWR characteristics**

V. Meunier et al.

[Title Page](#)[Abstract](#)[Introduction](#)[Conclusions](#)[References](#)[Tables](#)[Figures](#)[I◀](#)[▶I](#)[◀](#)[▶](#)[Back](#)[Close](#)[Full Screen / Esc](#)[Printer-friendly Version](#)[Interactive Discussion](#)

the K-band frequencies are the most affected (2.6 K in summer and  $-1.6$  K in winter at  $4^\circ$  and larger at lower elevations), because it is the only frequency band that is not nearly saturated at low elevation angles (Table 3). This effect also reduces at higher elevations angles as previously found by HW00. However, the information we can derive about this effect is limited because of the use of the climatological soundings and a climatological refractive index. The errors caused by the refractive index effects are smaller than those associated with the bandwidth effect for most frequencies (V and W band). The earth curvature yields under-estimation errors for all frequencies. This effect also has the greatest effect in K-band ( $-6.3$  K in winter and  $-5.5$  K in summer at  $4^\circ$  and larger at lower elevations) for the same reason as the refractive index effect (Table 3).

The present study is motivated by the increasing use of scanning radiometers, especially on the same scanner as a cloud or precipitation radar. Scanning radiometer measurements are important for temperature profile retrieval (Crewell and Löhnert, 2007) as well as for characterizing the spatial inhomogeneity of water vapor and liquid water field (Schween et al., 2011). The scanning radiometers are also being used in synergy with radars to provide additional information on the state of the atmosphere (Frisch et al., 1995; Saaverda et al., 2012; Löhnert et al., 2008; Westwater et al., 1983). The study illustrated that the beam widths errors are significant at low elevation where radars usually scan. Therefore, the beam width should be either taken account into the radiometer forward models or be physically reduced in the instruments for this use. When using the radar antenna for radiometer, the side lobes and absorption of the antenna are also factors to consider. For both instruments, averaging several points while scanning may cause smearing in the measurements. It was also found that, for most frequencies (except for V-band), increasing the bandwidth in order to compensate the reduce integration time cause by rapid scanning should not affect the radiometer sensitivity for bandwidth less than 1 GHz. However, the errors associated to the bandwidth are sounding dependent, and could lead to larger errors for certain atmospheric conditions.

**Biases caused by  
MWR characteristics**

V. Meunier et al.

[Title Page](#)[Abstract](#)[Introduction](#)[Conclusions](#)[References](#)[Tables](#)[Figures](#)[◀](#)[▶](#)[◀](#)[▶](#)[Back](#)[Close](#)[Full Screen / Esc](#)[Printer-friendly Version](#)[Interactive Discussion](#)

Retrieving atmospheric variables from radiometric measurements is a challenging task subject to large uncertainties. Part of the uncertainty is due to the physics of the interaction of the sensor with the atmosphere and its complexity. In order to minimize all other sources of uncertainty, a reliable instrument and forward model is required.

This study demonstrates that the inclusion of the instrument characteristics, the vertical gradients of refractive index and the earth curvature improves the forward modeling for radiances especially for low elevations.

*Acknowledgements.* This work was funded by the Natural Science and Engineering Research Council of Canada. The authors thank their colleagues from MWRnet for discussion leading to this paper at the EG-CLIMET Special Working Group workshop in Cologne.

**References**

Battaglia, A., Saaverdra Garfias, P., Rose, T., and Simmer, C.: Characterization of precipitating clouds by ground-based measurements with the triple-frequency polarized microwave radiometer ADMIRARI, *J. Appl. Meteorol. Clim.*, 49, 394–414, 2010.

Bean, B. R. and Dutton, E. J.: *Radio Meteorology*, US Government Printing Office, Washington, DC, USA, 1966.

Bianco, L., Cimini, D., Marzano, F. S., and Ware, R.: Combining microwave radiometer and wind profiler radar measurements for high-resolution atmospheric humidity profiling, *J. Atmos. Ocean. Tech.*, 22, 949–965, 2005.

Blahak, U.: An approximation to the effective beam weighting function for scanning meteorological radars with axisymmetric antenna patterns, *J. Atmos. Ocean. Tech.*, 25, 1182–1196, 2008.

Blaskovic, M., Bow, T. C., and Rogers, R. R.: *Radiometric Observations during CASP*, Montreal: Stormy Weather Group Scientific Report, McGill University, Montreal, Canada, 1987.

Cadeddu, M. P.: *Microwave Radiometer – High Frequency Handbook*, Office of Science, US Department of Energy, DOE/SC-ARM/TR-080, Washington, DC, USA, 2011.

Cadeddu, M. P.: *Microwave Radiometer – 3 channel (MWR3C) Handbook*, Office of Science, US Department of Energy, DOE/SC-ARM/TR-108, Washington, DC, USA, 2012.

**Biases caused by  
MWR characteristics**

V. Meunier et al.

Title Page

Abstract

Introduction

Conclusions

References

Tables

Figures

◀

▶

◀

▶

Back

Close

Full Screen / Esc

Printer-friendly Version

Interactive Discussion



Crewell, S. and Löhnert, U.: Accuracy of cloud liquid water path from ground-based microwave radiometry 2. sensor accuracy and synergy, *Radio Sci.*, 38, 8042, doi:10.1029/2002RS002634, 2003.

Crewell, S. and Löhnert, U.: Accuracy of Boundary layer temperature profiles retrieved with multifrequency multiangle microwave radiometry, *IEEE T. Geosci. Remote*, 45, 2195–2201, 2007.

Crewell, S., Czekala, H., Löhnert, U., Simmer, C., Rose, T., Zimmermann, R., and Zimmermann, R.: Microwave radiometer for cloud cartography: a 22-channel ground-based microwave radiometer for atmospheric research, *Radio Sci.*, 36, 621–638, 2001.

Doviak, R. J. and Zrnica, D. S.: *Doppler Radar and Weather Observations*, 2nd edn., Dover Publications Inc., Mineola, NY, USA, 2006.

Frisch, A. S., Fairall, C. W., and Snider, J. B.: Measurement of stratus cloud and drizzle parameters in ASTEX with a  $K_a$ -band Doppler radar and a microwave radiometer, *J. Atmos. Sci.*, 52, 2788–2799, 1995.

Gaffard, C., Hewison, T., and Nash, J.: Toward the combination of active and passive remote sensors for temperature and humidity profiling, 6th International Symposium on Tropospheric Profiling, 59, Leipzig, Germany, 14–20 June, 2003.

Gaikovich, K. P.: *Inverse problems in physical diagnostics*, Nova Science Publishers Inc., Hauppauge, NY, USA, 2004.

Göldner, J. and Spänkuch, D.: Results of a year-round remotely sensed integrated water vapor by ground-based microwave radiometry, *J. Appl. Meteorol. Clim.*, 38, 981–988, 1999.

Han, Y. and Westwater, E. R.: Analysis and improvement of tipping calibration for ground-based microwave radiometers, *IEEE T. Geosci. Remote*, 38, 1260–1276, 2000.

Huang, D., Liu, Y., and Wiscombe, W.: Determination of cloud liquid water distribution using 3-D cloud tomography, *J. Geophys. Res.-Atmos.*, 113, 13201, doi:10.1029/2007JD009133, 2008.

Kipp and Zonen: MTP5: air temperature profiles by microwave technologies, available at: <http://www.kippzonen.com/?downloadcategory/65162/Discontinued+MTP+5.aspx> (last access: 16 January 2012), 2012.

Liljegren, J. C.: *Microwave radiometer profiler handbook: evaluation of a new multi-frequency microwave radiometer for measuring the vertical distribution of temperature, water vapor, and cloud liquid water*, DOE Atmospheric Radiation Measurement (ARM) Program, Argonne National Lab., Argonne, IL, USA, 2002.

**Biases caused by  
MWR characteristics**

V. Meunier et al.

Title Page

Abstract

Introduction

Conclusions

References

Tables

Figures

◀

▶

◀

▶

Back

Close

Full Screen / Esc

Printer-friendly Version

Interactive Discussion



- Löhnert, U. and Crewell, S.: Accuracy of cloud liquid water path from ground-based microwave radiometry 1. dependency on cloud model statistics, *Radio Sci.*, 38, 8041, doi:10.1029/2002RS002654, 2003.
- Löhnert, U., Crewell, S., Krasnov, O., O'Connor, E., and Russchenberg, H.: Advances in continuously profiling the thermodynamic state of the boundary layer: integration of measurements and methods, *J. Atmos. Ocean. Tech.*, 25, 1251–1266, 2008.
- Martin, L., Schneebeli, M., and Mätzler, C.: Tropospheric water and temperature retrieval for ASMUWARA, *Meteorol. Z.*, 15, 37–44, 2006a.
- Martin, L., Schneebeli, M., and Mätzler, C.: ASMUWARA, a ground-based radiometer system for tropospheric monitoring, *Meteorol. Z.*, 15, 11–17, 2006b.
- McClatchey, R. A., Fenn, R. W., Selby, J. E. A., Volz, F. E., and Garing, J. S.: Optical properties of the atmosphere, Tech. Rep. AFCRL-72-0497, Air Force Cambridge Research Laboratory, Hanscom Air Force Base, Bedford, MA, USA, 1971.
- Padmanabhan, S., Reising, S. C., Vivekanandan, J., and Iturbide-Sanchez, F.: Retrieval of atmospheric water vapor density with fine spatial resolution using three-dimensional tomographic inversion of microwave brightness temperatures measured by a network of scanning compact radiometers, *IEEE T. Geosci. Remote*, 47, 3708–3721, 2009.
- Petty, G. W.: *A First Course in Atmospheric Radiation*, 2nd Edn., Sundog Publishing, Madison, WI, USA, 2006.
- Radiometer Physics GmbH: Profiling Radiometers: HATPRO/ HUMPRO/ TEMPRO series, available at: [http://www.radiometer-physics.de/rpg/html/docs/RPG\\_MWR\\_PRO\\_TN.pdf](http://www.radiometer-physics.de/rpg/html/docs/RPG_MWR_PRO_TN.pdf) (last access: 19 August 2010), 2010.
- Rose, T., Crewell, S., Löhnert, U., and Simmer, C.: A network suitable microwave radiometer for operational monitoring of the cloudy atmosphere, *Atmos. Res.*, 75, 183–200, 2005.
- Rosenkranz, P. W.: Water vapor microwave continuum absorption: a comparison of measurements and models, *Radio Sci.*, 33, 919–928, 1998.
- Rüeger, J. M.: Refractive index formulae for radio waves, in: *Integration of Techniques and Corrections to Achieve Accurate Engineering*, Proc. XXII FIG Int. Congress ACSM/SPRS Ann. Conf., Washington DC, USA, 19–26 April, JS28, 2002.
- Saavedra, P., Battaglia, A., and Simmer, C.: Partitioning of cloud water and rainwater content by ground-based observations with the Advanced Microwave Radiometer for Rain Identification (ADMIRARI) in synergy with a micro rain radar, *J. Geophys. Res.*, 117, D05203, doi:10.1029/2011JD016579, 2012.

**Biases caused by  
MWR characteristics**

V. Meunier et al.

[Title Page](#)[Abstract](#)[Introduction](#)[Conclusions](#)[References](#)[Tables](#)[Figures](#)[◀](#)[▶](#)[◀](#)[▶](#)[Back](#)[Close](#)[Full Screen / Esc](#)[Printer-friendly Version](#)[Interactive Discussion](#)

- Schween, J. H., Crewell, S., and Löhnert, U.: Horizontal-humidity gradient from one single-scanning microwave radiometer, *IEEE Geosci. Remote S.*, 8, 336–340, 2011.
- Shupe, M. D., Daniels, J. S., de Boer, G., Eloranta, E. W., Kollias, P., Long, C. N., Luke, E. P., Turner, D. D., and Verlinde, J.: A focus on mixed-phase clouds: the status of ground-based observational methods, *B. Am. Meteorol. Soc.*, 89, 1549–1562, 2008.
- 5 Staelin, D. H.: Measurements and interpretation of the microwave spectrum of the terrestrial atmosphere near 1-cm wavelength, *J. Geophys. Res.*, 71, 2875–2881, 1966.
- Ulaby, F. T., Moore, R. K., and Fung, A. K., *Microwave Remote Sensing: Active and Passive, Vol. I – Microwave Remote Sensing Fundamentals and Radiometry*, Arctech House, Norwood, MA, USA, 1981.
- 10 Voyles, J. W.: ARM Climate Research Facility Quaterly Instrument Report, Forth quarter: 1 October–30 December, 2010, Office of Science, US Department of Energy, DOE/SC-ARM-11-001, Washington, DC, USA, 2011.
- Ware, R., Carpenter, R., Güldner, J., Liljegren, J. C., Nehrkom, T., Solheim, F., and Vandenberghe, F.: A multichannel radiometric profiler of temperature, humidity and cloud liquid, *Radio Sci.*, 38, 8079, doi:10.1029/2002RS002856, 2003.
- 15 Westwater, E. R., Decker, M. T., Zachs, A., and Gage, K. S.: Ground-based remote sensing of temperature profiles by a combination of microwave radiometry and radar. *J. Clim. Appl. Meteorol.*, 22, 126–133, 1983.

**Biases caused by  
MWR characteristics**

V. Meunier et al.

Title Page

Abstract

Introduction

Conclusions

References

Tables

Figures

◀

▶

◀

▶

Back

Close

Full Screen / Esc

Printer-friendly Version

Interactive Discussion

**Table 1.** A sample of current commercial and experimental radiometers that inspired the instrument design characteristics included in this study, where HPFW is half power full width.

Radiometer name	Beam width (HPFW)	Bandwidth	Frequency bands	References
ADMIRARI	5°–6.53°	400 MHz	X and K band (3 frequencies)	Battaglia et al. (2010)
ASMUWARA	7.9°–10°	300–4000 MHz	K, V, mm bands and IR (9 frequencies)	Martin et al. (2006b)
HATPRO	2.5°–3.5°	100–2000 MHz	K and V band (14 frequencies)	Rose et al. (2005) Radiometer Physic GmbH (2010)
LWP-90-150	1.5°–1.8°	2000 MHz	W and D band (2 frequencies)	Cadeddu (2011)
MWR3C	3.0°–3.5°	300 MHz – 1900 MHz	K and W band (3 frequencies)	Cadeddu (2012)
MICCY	0.4°–0.9°	250–1000 MHz	K, V, and W band (22 frequencies)	Crewell et al. (2001)
MP-3000A	2.2°–6.1°	400 MHz	K and V band (12 frequencies)	Liljgren (2002) Ware et al. (2003)
MTP-5	< 0.9°–3°	~ 4000 MHz	V band (1 frequency)	Kipp and Zonen (2012) Gaikovich (2004)

**Biases caused by  
MWR characteristics**

V. Meunier et al.

Title Page

Abstract

Introduction

Conclusions

References

Tables

Figures

◀

▶

◀

▶

Back

Close

Full Screen / Esc

Printer-friendly Version

Interactive Discussion

**Table 2.** Summary of the instrument characteristics included in the study.

Frequencies	K-band (15–35 GHz), V-band (50–60 GHz), W-band (94–95.5 GHz),
Bandwidths (MHz)	100, 200, 300, 400, 500, 600, 700, 800, 900, 1000
Beam width (°)	0.5, 1, 2, 3, 4, 5, 6, 7, 8, 9, 10
Elevation angles (°)	0.5, 2, 4, 6, 8, 10, 12, 14, 20, 25, 30, 45, 60, 90

**Biases caused by  
MWR characteristics**

V. Meunier et al.

**Table 3.** Summary of the range of biases for elevation angles above  $4^\circ$  in TB (in K) associated to each effect (bandwidth (100–1000 MHz), beam width ( $0.5\text{--}10^\circ$ ), refractivity, and earth curvature) for each set of frequencies and each sounding. Entries with long dashes represent values that are below any instrument measurement capability.

	Mid-latitude summer		Mid-latitude winter	
	Maximum	Minimum	Maximum	Minimum
Bandwidth K-band	1.8	–0.8	1.6	–0.6
Bandwidth V-Band	7.9	–2.2	6.5	–1.9
Bandwidth W-Band	0	–	0	–
Beam width K-band	13.2	–40.3	–0.01	–34.5
Beam width V-band	8	–2.2	8.1	–2.2
Beam width W-band	10.9	–2.9	3.6	–9.3
Refractivity K-band	2.6	0	0	–1.6
Refractivity V-band	–	–	0	–0.1
Refractivity W-band	–	0	0	–0.3
Curvature K-band	0	–5.5	0	–6.3
Curvature V-band	0	–1.2	0	–1.2
Curvature W-band	0	–0.9	0	–45

Title Page

Abstract

Introduction

Conclusions

References

Tables

Figures

◀

▶

◀

▶

Back

Close

Full Screen / Esc

Printer-friendly Version

Interactive Discussion



## Biases caused by MWR characteristics

V. Meunier et al.

**Table 4.** Summary of retrieval errors associated to the different effects (bandwidth (100–1000 MHz), beam width (0.5–10°)) for each retrieval parameter IWV(kg m<sup>-2</sup>), LWP(gm<sup>-2</sup>) and temperature (K) for each sounding. Entries with long dashes represent values that are below any instrument measurement capability.

	Mid-latitude summer		Mid-latitude winter	
	Maximum	Minimum	Maximum	Minimum
IWV bandwidth (kg m <sup>-2</sup> )	0	-0.7	0	-0.5
IWV beam width (kg m <sup>-2</sup> )	5.3	0	7.9	0
LWP bandwidth (gm <sup>-2</sup> )	–	0	–	0
LWP beam width (gm <sup>-2</sup> )	32	0	9	0
T bandwidth (K)	0.7	-1.8	0.7	-1.8
T beam width (K)	0.2	–	0.2	–

[Title Page](#)
[Abstract](#)
[Introduction](#)
[Conclusions](#)
[References](#)
[Tables](#)
[Figures](#)
[I◀](#)
[▶I](#)
[◀](#)
[▶](#)
[Back](#)
[Close](#)
[Full Screen / Esc](#)
[Printer-friendly Version](#)
[Interactive Discussion](#)


**Biases caused by  
MWR characteristics**

V. Meunier et al.

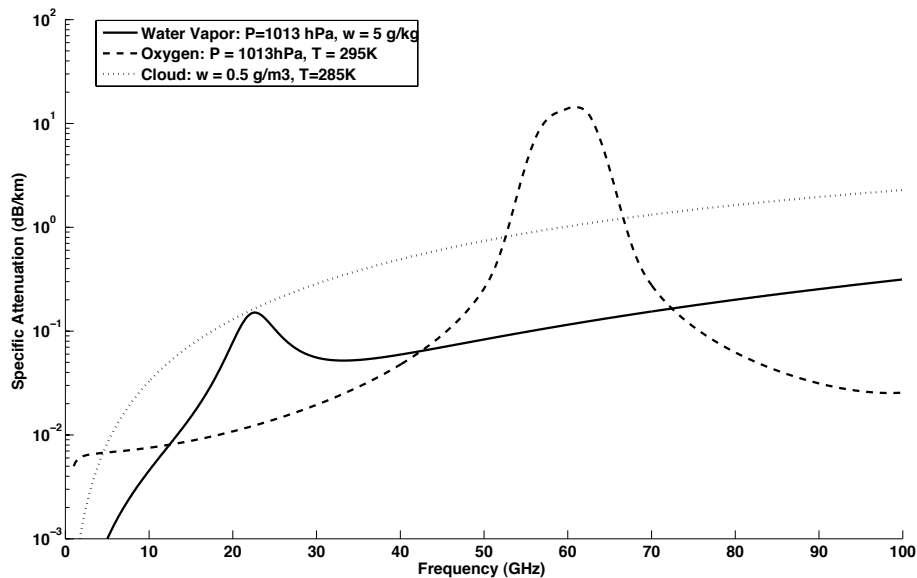


**Fig. 1.** One-way specific attenuation curves of water vapor (dashed), oxygen (line) and cloud (dotted) in  $\text{dB km}^{-1}$ .

[Title Page](#)[Abstract](#)[Introduction](#)[Conclusions](#)[References](#)[Tables](#)[Figures](#)[◀](#)[▶](#)[◀](#)[▶](#)[Back](#)[Close](#)[Full Screen / Esc](#)[Printer-friendly Version](#)[Interactive Discussion](#)

**Biases caused by  
MWR characteristics**

V. Meunier et al.

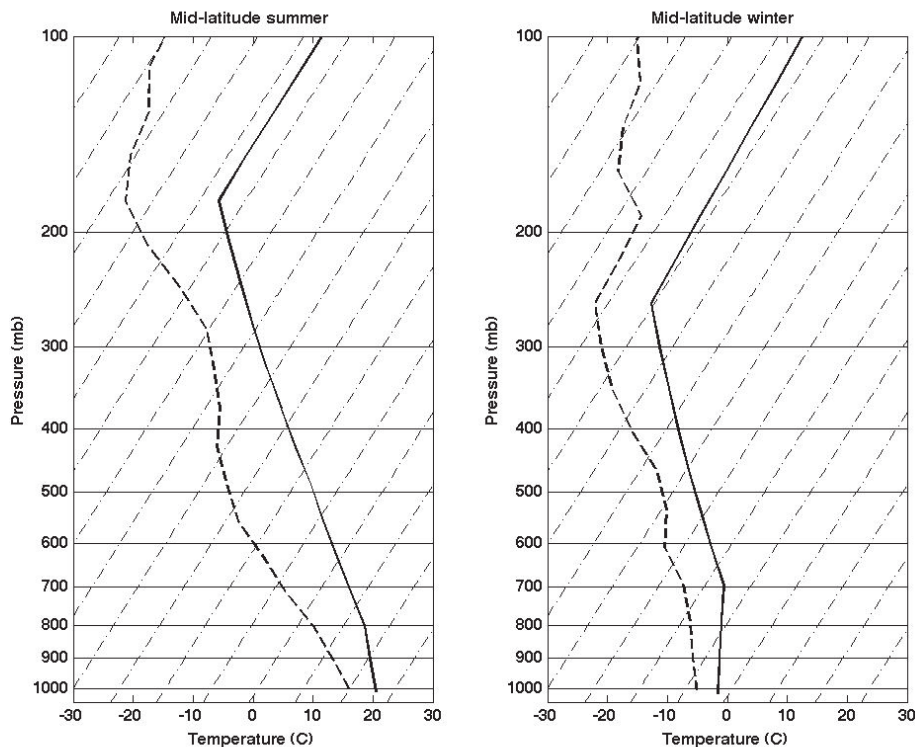


**Fig. 2.** The McClatchey climatological soundings (in skew-T plots) used in this study mid-latitude summer (left) and winter (right). In these plots, temperature is in full line, dew point temperature is in dashed.

[Title Page](#)[Abstract](#)[Introduction](#)[Conclusions](#)[References](#)[Tables](#)[Figures](#)[◀](#)[▶](#)[◀](#)[▶](#)[Back](#)[Close](#)[Full Screen / Esc](#)[Printer-friendly Version](#)[Interactive Discussion](#)

**Biases caused by  
MWR characteristics**

V. Meunier et al.

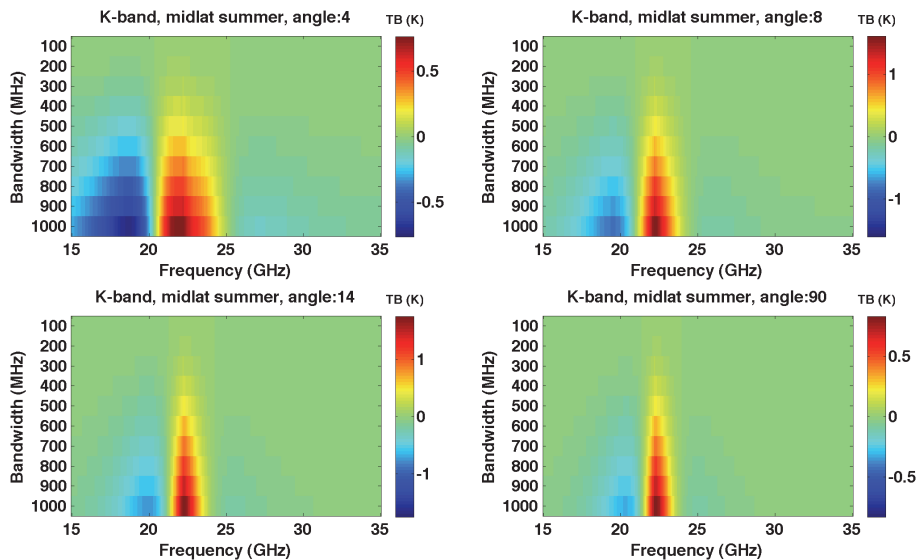


**Fig. 3.** The errors associated to the channel bandwidth effect in TB differences for K-band frequencies using the mid-latitude summer atmospheric profile. The TB differences are defined as the TB calculated from a forward model without bandwidth minus the TB calculated from a forward model with bandwidth.

Title Page

Abstract

Introduction

Conclusions

References

Tables

Figures

◀

▶

◀

▶

Back

Close

Full Screen / Esc

Printer-friendly Version

Interactive Discussion



Biases caused by  
MWR characteristics

V. Meunier et al.

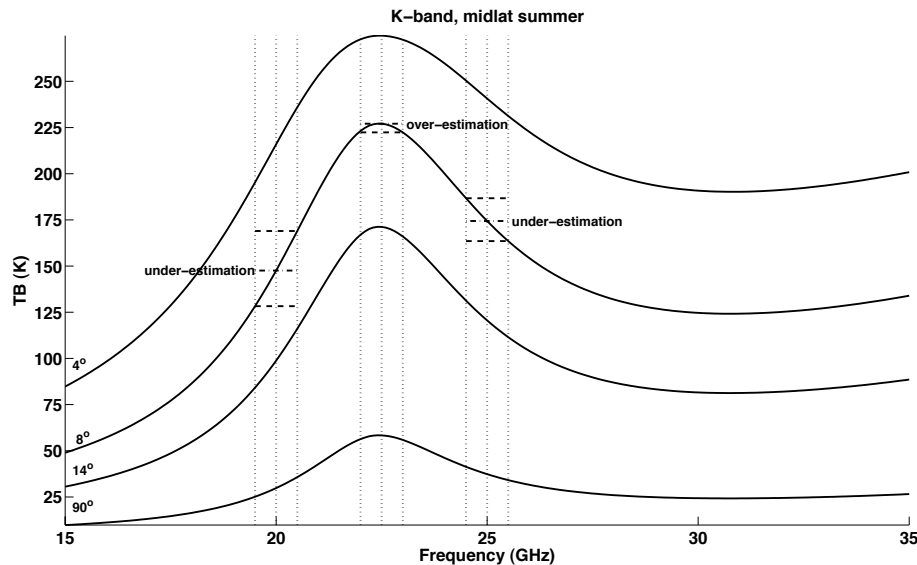


**Fig. 4.** Explanation of over and under estimations that cause the bandwidth errors, which are linked to the curvature of the TB vs frequency curve in K-band for the mid-latitude summer sounding. The vertical dotted lines represent the 1 GHz bandwidth (center line is center frequency). The short horizontal dashed lines are used to locate the intersection of the extremities of the bandwidth and the dashed dot line locates the center frequency on the TB curve. These additional lines help to visually see that the over-estimation and under-estimation errors are linked to the curvature of the TB curve.

Title Page

Abstract

Introduction

Conclusions

References

Tables

Figures

◀

▶

◀

▶

Back

Close

Full Screen / Esc

Printer-friendly Version

Interactive Discussion



Biases caused by  
MWR characteristics

V. Meunier et al.

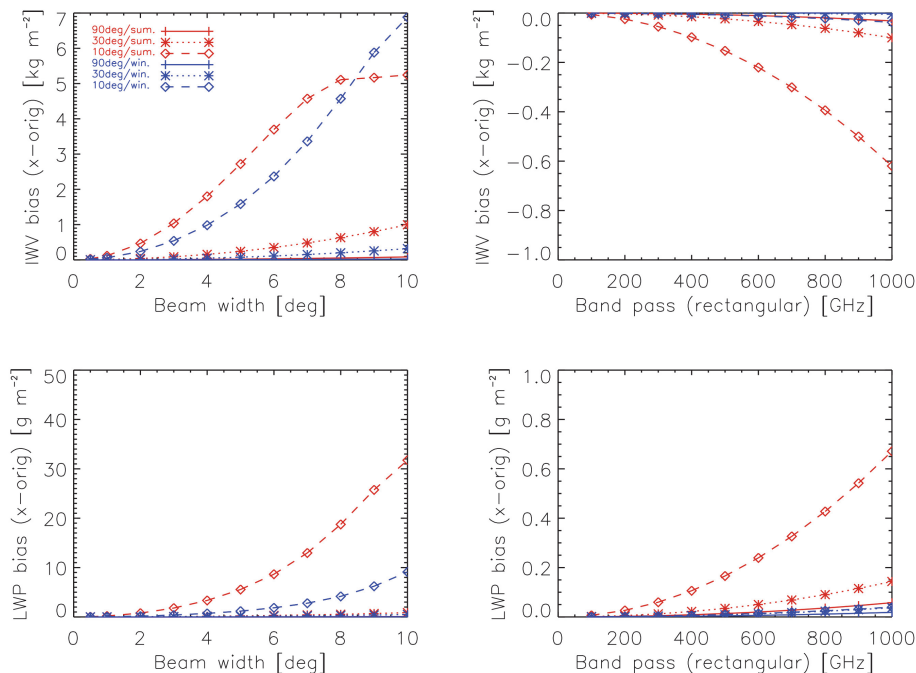


**Fig. 5.** The error in the retrieved IWV (in  $\text{kg m}^{-2}$ ) and LWP (in  $\text{g m}^{-2}$ ) caused by the errors in TB by not taking into account antenna beam width (right) or bandwidth (left). The errors are shown for both the mid-latitude summer (red) and the mid-latitude winter soundings (blue) for elevation angles  $10^\circ$  (dash square),  $30^\circ$  (dot star), and  $90^\circ$  (line +).

Title Page

Abstract

Introduction

Conclusions

References

Tables

Figures

◀

▶

◀

▶

Back

Close

Full Screen / Esc

Printer-friendly Version

Interactive Discussion



Biases caused by  
MWR characteristics

V. Meunier et al.

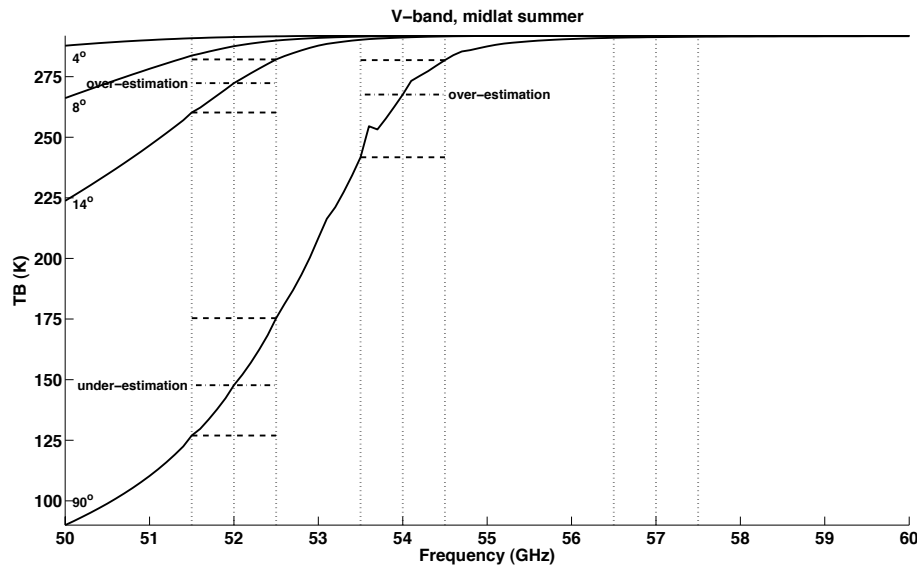


**Fig. 6.** Explanation of over and under estimations that cause the bandwidth errors, which are linked to the curvature of the TB vs frequency curve in V-band for the mid-latitude summer sounding. The vertical dotted lines represent the 1 GHz bandwidth (center line is center frequency). The short horizontal dashed lines are used to locate the intersection of the extremities of the bandwidth and the dashed dot line locates the center frequency on the TB curve. These additional lines help to visually see that the over-estimation and under-estimation errors are linked to the curvature of the TB curve.

Title Page

Abstract

Introduction

Conclusions

References

Tables

Figures

◀

▶

◀

▶

Back

Close

Full Screen / Esc

Printer-friendly Version

Interactive Discussion



**Biases caused by  
MWR characteristics**

V. Meunier et al.

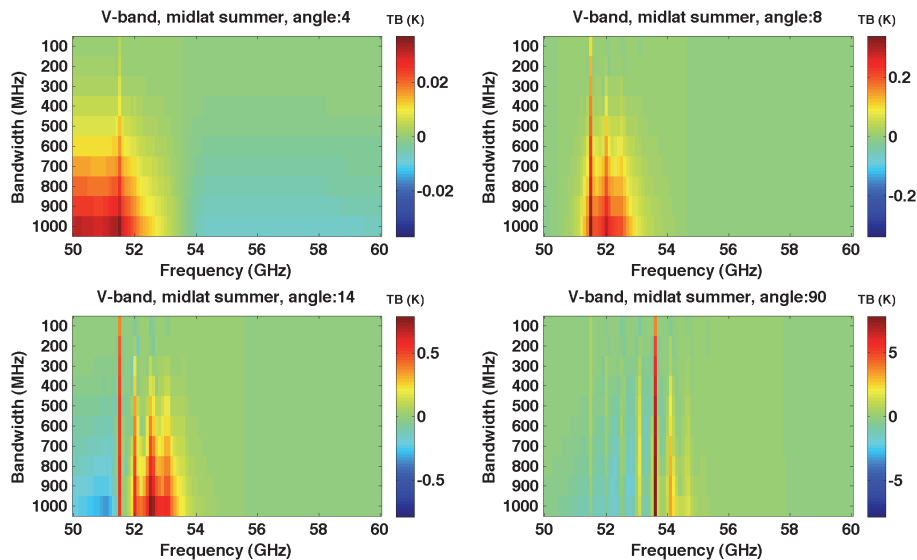


**Fig. 7.** The errors associated to the channel bandwidth effect in differential TB for V-band frequencies using the mid-latitude summer atmospheric profile. The TB differences are defined as the TB calculated from a forward model without bandwidth minus the TB calculated from a forward model with bandwidth.

[Title Page](#)[Abstract](#)[Introduction](#)[Conclusions](#)[References](#)[Tables](#)[Figures](#)[◀](#)[▶](#)[◀](#)[▶](#)[Back](#)[Close](#)[Full Screen / Esc](#)[Printer-friendly Version](#)[Interactive Discussion](#)

## Biases caused by MWR characteristics

V. Meunier et al.

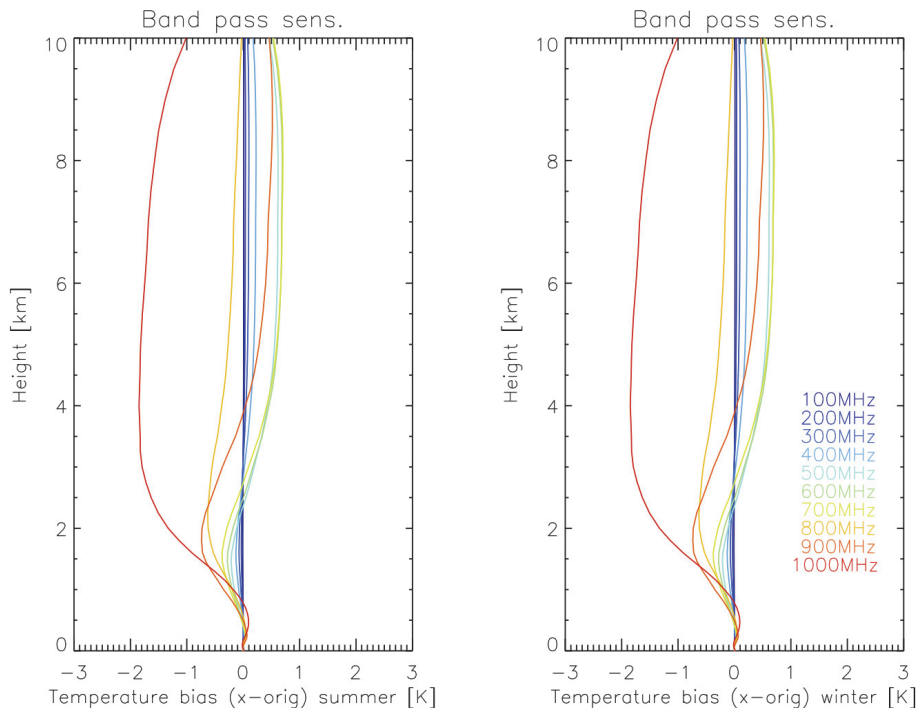


**Fig. 8.** The error in the retrieved temperature caused by the errors in TB by not taking into account channel bandwidth for different level in the atmosphere. The errors are shown for both the mid-latitude summer (right) and the mid-latitude winter (left) soundings for different bandwidths (color scale).

Title Page

Abstract

Introduction

Conclusions

References

Tables

Figures

◀

▶

◀

▶

Back

Close

Full Screen / Esc

Printer-friendly Version

Interactive Discussion



**Biases caused by  
MWR characteristics**

V. Meunier et al.

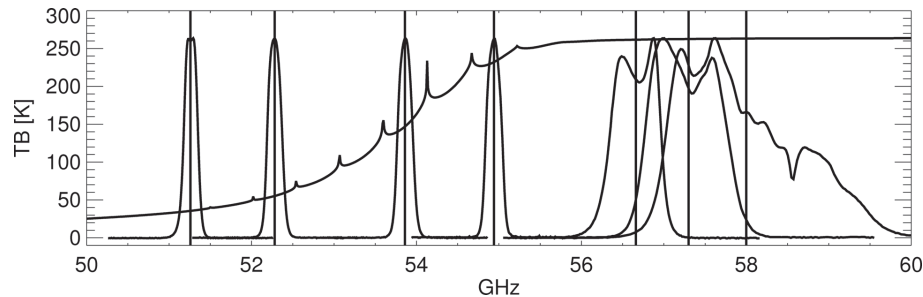


**Fig. 9.** The oxygen absorption complex at V-band. Notice individual absorption peaks that are resolved. Also plotted are the HATPRO radiometer V-band channels and their respective bandwidths. The TB spectrum plotted here was made using a sounding from RHUBC-II in Chile (5322 m ABSL). (G. Maschwitz, personal communication, June 2012.)

[Title Page](#)[Abstract](#)[Introduction](#)[Conclusions](#)[References](#)[Tables](#)[Figures](#)[◀](#)[▶](#)[◀](#)[▶](#)[Back](#)[Close](#)[Full Screen / Esc](#)[Printer-friendly Version](#)[Interactive Discussion](#)

**Biases caused by  
MWR characteristics**

V. Meunier et al.

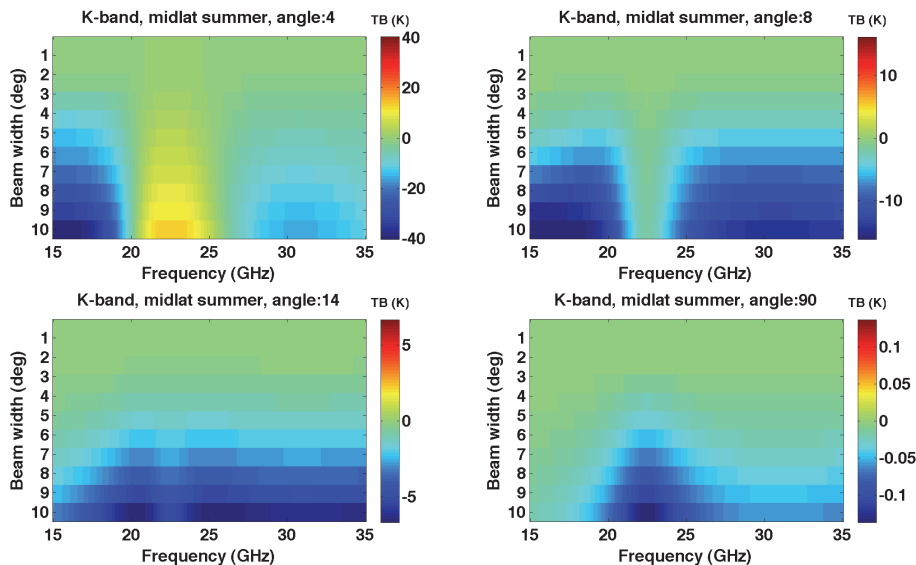


**Fig. 10.** The errors associated to the antenna beam width effect in fractional opacity for K-band frequencies using the mid-latitude summer atmospheric profile. The TB differences are defined as the TB calculated from a forward model without beam width minus the TB calculated from a forward model with beam width.

[Title Page](#)[Abstract](#)[Introduction](#)[Conclusions](#)[References](#)[Tables](#)[Figures](#)[◀](#)[▶](#)[◀](#)[▶](#)[Back](#)[Close](#)[Full Screen / Esc](#)[Printer-friendly Version](#)[Interactive Discussion](#)

## Biases caused by MWR characteristics

V. Meunier et al.

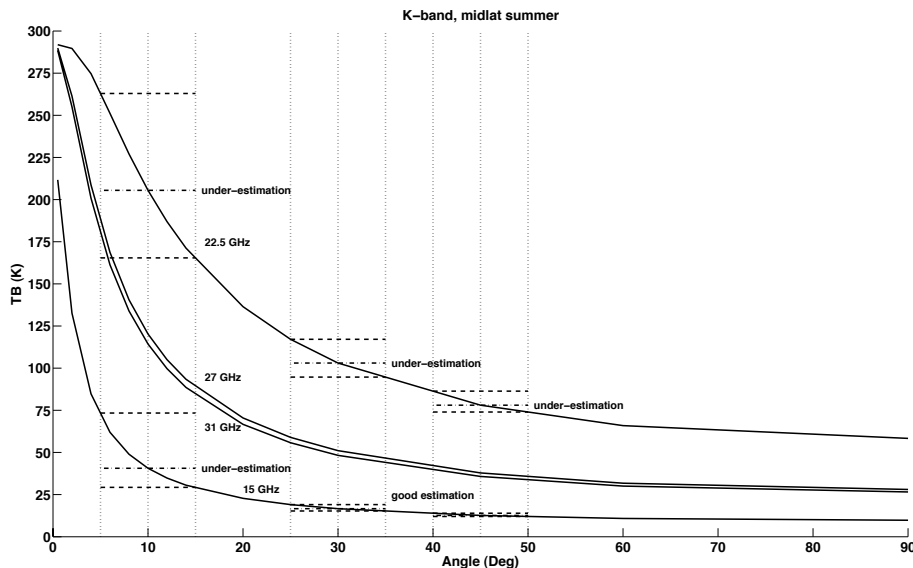


**Fig. 11.** Explanation of over and under estimations that cause the beam width errors, which are linked to the curvature of the TB vs angle curve in K-band for the mid-latitude summer sounding. The vertical dotted lines represent the  $10^\circ$  beam width (center line is center angle). The short horizontal dashed lines are used to locate the intersection of the extremities of the beam width and the dashed dot line locates the center angle on the TB curve. These additional lines help to visually see that the over-estimation and under-estimation errors are linked to the curvature of the TB curve.

Title Page

Abstract

Introduction

Conclusions

References

Tables

Figures

◀

▶

◀

▶

Back

Close

Full Screen / Esc

Printer-friendly Version

Interactive Discussion



Biases caused by  
MWR characteristics

V. Meunier et al.

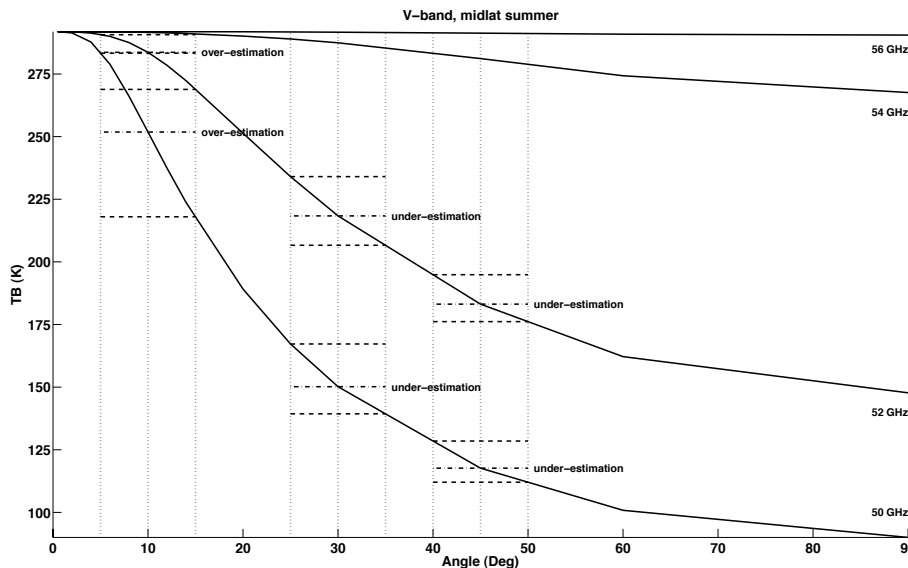


**Fig. 12.** Explanation of over and under estimations that cause the beam width errors, which are linked to the curvature of the TB vs angle curve in V-band for the mid-latitude summer sounding. The vertical dotted lines represent the  $10^\circ$  beam width (center line is center angle). The short horizontal dashed lines are used to locate the intersection of the extremities of the beam width and the dashed dot line locates the center angle on the TB curve. These additional lines help to visually see that the over-estimation and under-estimation errors are linked to the curvature of the TB curve.

[Title Page](#)
[Abstract](#)
[Introduction](#)
[Conclusions](#)
[References](#)
[Tables](#)
[Figures](#)
[◀](#)
[▶](#)
[◀](#)
[▶](#)
[Back](#)
[Close](#)
[Full Screen / Esc](#)
[Printer-friendly Version](#)
[Interactive Discussion](#)


**Biases caused by  
MWR characteristics**

V. Meunier et al.

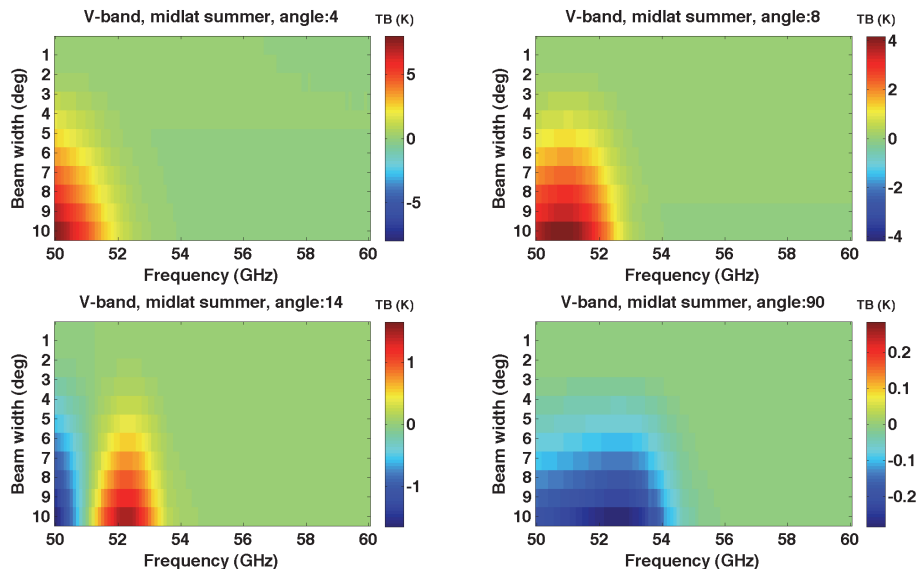


**Fig. 13.** The errors associated to the antenna beam width effect in differential TB for V-band frequencies using the mid-latitude summer atmospheric profile. The TB differences are defined as the TB calculated from a forward model without beam width minus the TB calculated from a forward model with beam width.

Title Page

Abstract

Introduction

Conclusions

References

Tables

Figures

◀

▶

◀

▶

Back

Close

Full Screen / Esc

Printer-friendly Version

Interactive Discussion



**Biases caused by  
MWR characteristics**

V. Meunier et al.

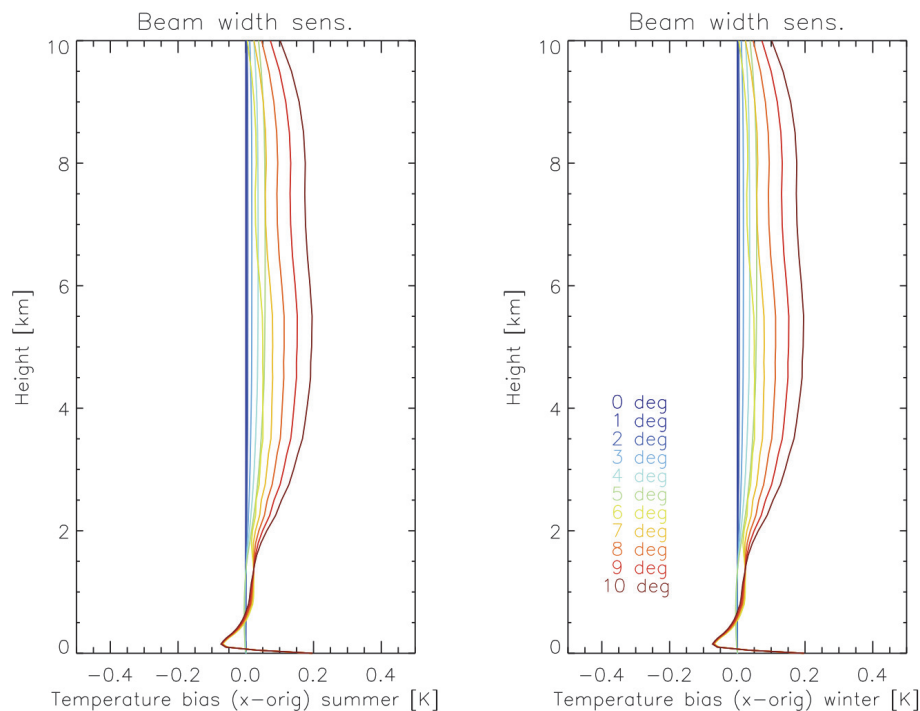


**Fig. 14.** The error in the retrieved temperature caused by the errors in TB by not taking into account antenna beam width for different level in the atmosphere. The errors are shown for both the mid-latitude summer (right) and the mid-latitude winter (left) soundings for different beam widths (color scale).

[Title Page](#)[Abstract](#)[Introduction](#)[Conclusions](#)[References](#)[Tables](#)[Figures](#)[◀](#)[▶](#)[◀](#)[▶](#)[Back](#)[Close](#)[Full Screen / Esc](#)[Printer-friendly Version](#)[Interactive Discussion](#)

**Biases caused by  
MWR characteristics**

V. Meunier et al.

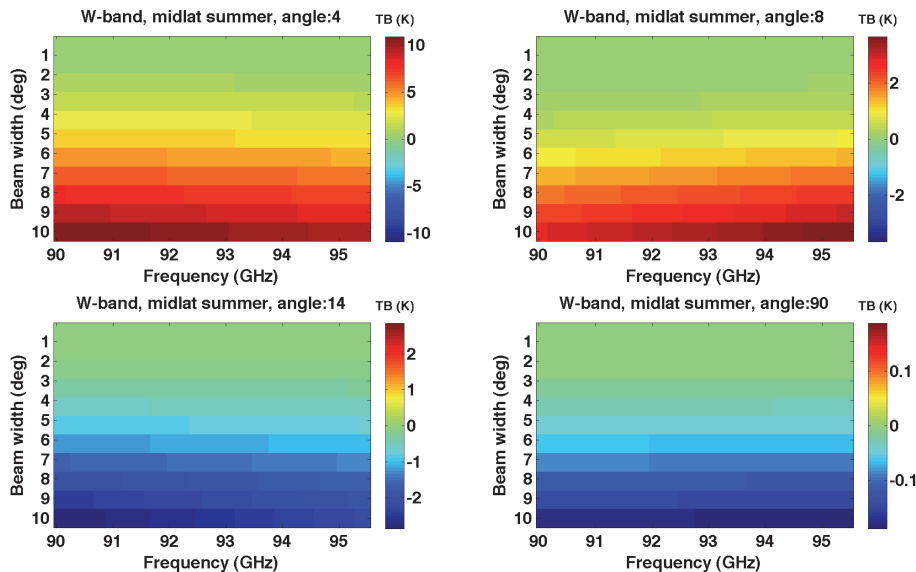


**Fig. 15.** The errors associated to the antenna beam width effect in differential TB for W-band frequencies using the mid-latitude summer atmospheric profile. The TB differences are defined as the TB calculated from a forward model without beam width minus the TB calculated from a forward model with beam width.

Title Page

Abstract

Introduction

Conclusions

References

Tables

Figures

◀

▶

◀

▶

Back

Close

Full Screen / Esc

Printer-friendly Version

Interactive Discussion



Biases caused by  
MWR characteristics

V. Meunier et al.

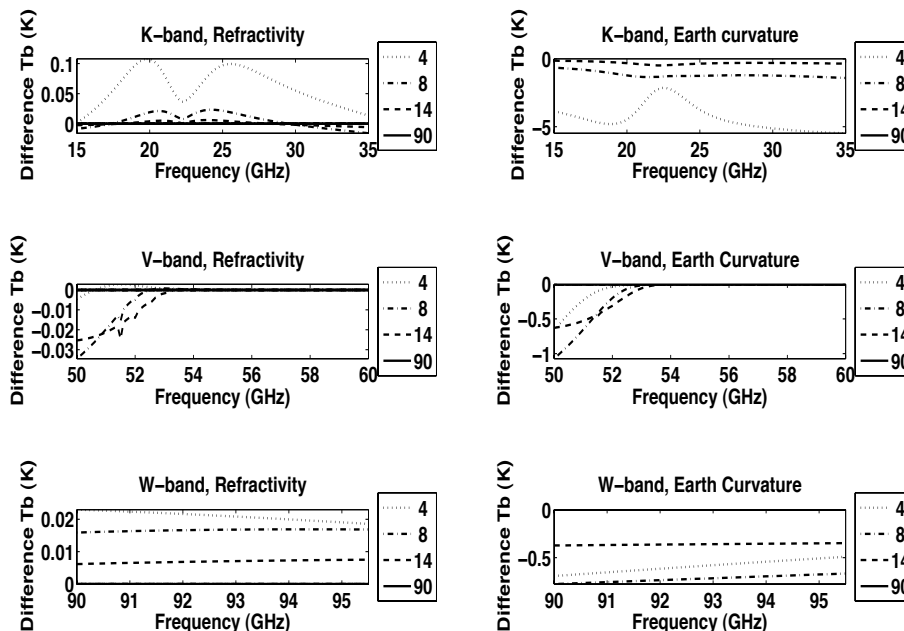


**Fig. 16.** The errors in TB associated to the refractivity effect on the left column and the earth curvature effect on the right column at all frequencies for the mid-latitude summer profile in TB differences. The top plots show the results for K-band, the middle ones are V-band, and the bottom ones are W-band. In all plots, the dashed line is 4° elevation, dotted line is 8°, dash dot line is 14°, and the full line is 90°.

Title Page

Abstract

Introduction

Conclusions

References

Tables

Figures

◀

▶

◀

▶

Back

Close

Full Screen / Esc

Printer-friendly Version

Interactive Discussion

